ACS SyntheticBiology

pubs.acs.org/synthbio

Research Article

Oncogenic Alterations in PI3K Signaling Emulated Optogenetically Recapitulate Some Phenotypic Changes in Mammary Epithelia

Keith A. Gagnon, Veronica W. Hui, Terry Ching, Amy E. Stoddard, Esther Koh, Jeroen Eyckmans, Ahmad S. Khalil,* and Christopher S. Chen*

Cite This: https://doi.org/10.1021/acssynbio.5c00651

Read Online

ACCESS | Metrics & More | Article Recommendations | Supporting Information

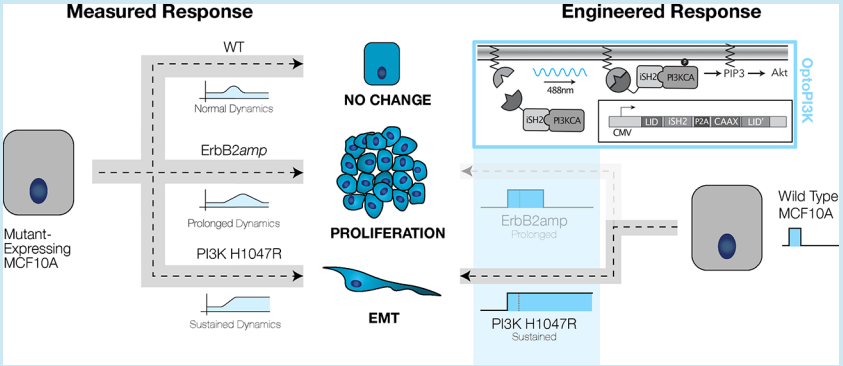

ABSTRACT: Cancer is known to be a disease of altered cellular signaling; however, the relationship between mutation-specific changes to signal transduction and the phenotypic consequences produced remains poorly understood. Here, we investigate two common breast cancer driver mutations, the *PIK3CA*^{H1047R} mutation and the *ErbB2* amplification, both of which activate the PI3K-Akt pathway but paradoxically drive distinct cellular outcomes. Indeed, in nontransformed mammary epithelial cells, PI3K^{H1047R} expression induced features of epithelial−mesenchymal transition (EMT), while ErbB2^{amp} cells exhibited a hyperproliferative phenotype. Characterization of PI3K axis signaling revealed that ErbB2^{amp} cells display prolonged, stimulus-dependent PI3K activation, whereas PI3K^{H1047R} cells show constitutive, ligand-independent signaling. To test whether these distinct dynamics contribute to the phenotypic responses, we employed an iLID-based optogenetic system that enables precise, tunable control of endogenous PI3K activity. Using this tool to mimic the mutation-specific dynamics in MCF10A mammary epithelial cells, we found that PI3K signaling patterns alone were sufficient to reproduce key features of the *PIK3CA H1047R*-associated EMT phenotype but not the *ErbB2*-associated proliferative phenotype. These findings suggest that the temporal encoding of pathway activity, not merely its magnitude, can drive some phenotypic changes in oncogenic progression, explain how distinct mutations within a common signaling pathway can produce divergent cellular phenotypes, and provide a workflow for interrogating the functional consequences of changes in signaling dynamics.

KEYWORDS: *optogenetics, PI3K-signaling, breast cancer, EMT, temporal dynamics, signaling dynamics*

INTRODUCTION

Cells interpret and respond to soluble ligands primarily through transmembrane receptors that, upon ligand binding, initiate intracellular signaling cascades to drive context-specific changes in gene expression and cellular behavior.[1,2] Although hundreds of distinct ligand−receptor pairs exist, each driving distinct changes to cellular behavior, the intracellular signaling machinery used in each case is funneled through a limited set of canonical pathways. This apparent discrepancy raises a fundamental question: how do cells discriminate between different extracellular cues when signaling is routed through shared transduction axes? Recent work has suggested that one mechanism for such regulation is the temporal encoding of ligand identity into canonical pathway activity.[3−5] Biological signals exhibit time-variant characteristics, and temporal features, including signal duration, intensity, and frequency, have all emerged as key regulators of cellular decision-making.[6−8] This has been demonstrated most convincingly within the MAPK pathway, where temporal dynamics have been shown to regulate proliferation, differentiation, and apoptosis.[9−11] Given the role of MAPK in these varied and

Received: September 1, 2025
Revised: December 23, 2025
Accepted: January 6, 2026

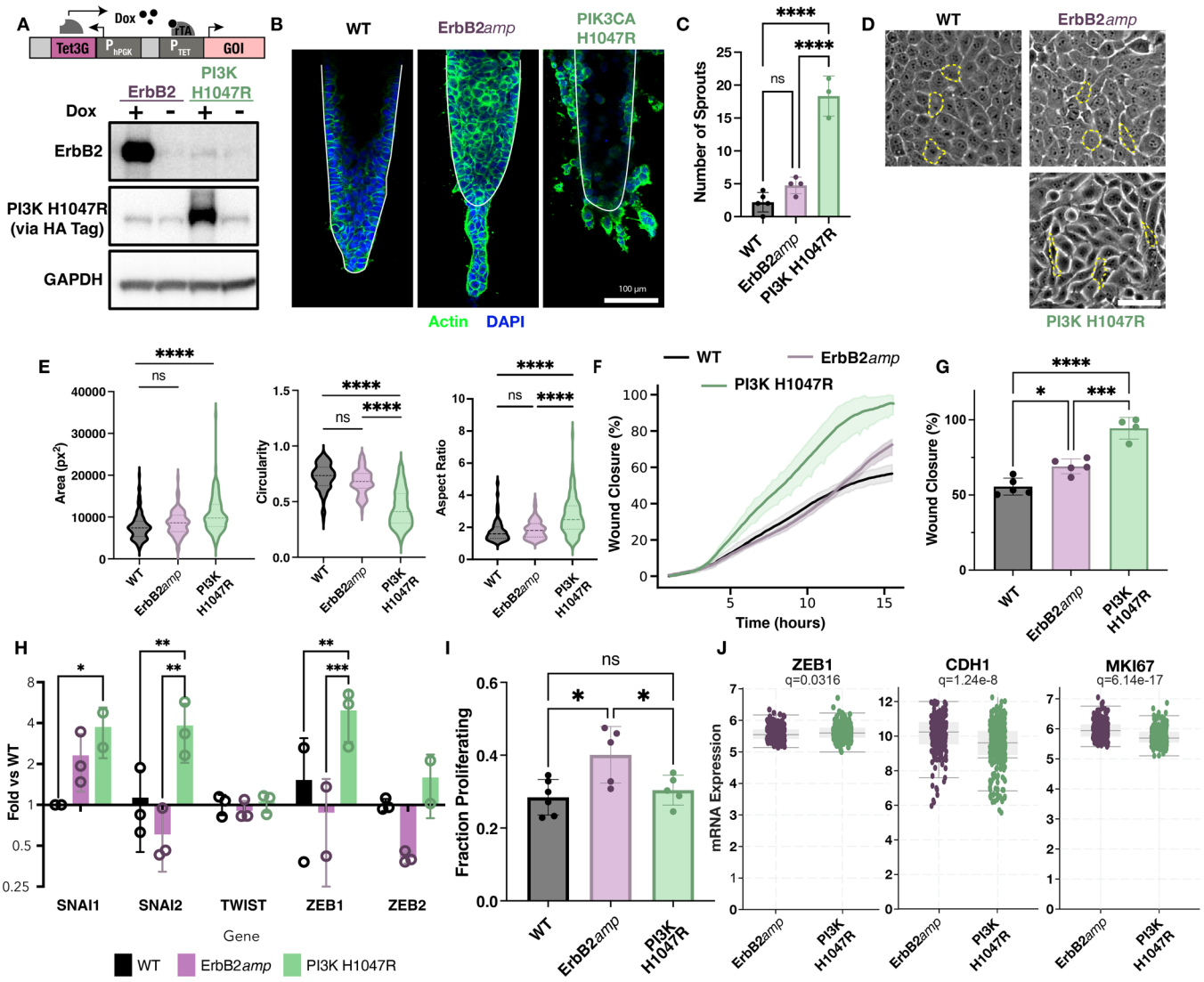

Figure 1. ErbB2^{amp} and the PI3K^{H1047R} mutation drive distinct cellular responses in MCF10A mammary epithelium. (A) Western blot of MCF10A lysate showing expression of ErbB2 or PI3K H1047R in response to doxycycline. (Upper) Schematic showing doxycycline-inducible expression circuit. (B) Representative bioengineered mammary ducts seeded with either WT, ErbB2^{amp}, or PI3K^{H1047R} expressing MCF10A. (C) Quantification of the number of invasive sprouts per duct (n = 3−5 devices per condition). (D) 2D phase contrast images showing morphology of cells expressing either mutation. Representative cells outlined for clarity. Scale bar = 25 μm. (E) Quantification of cell area (left), circularity (middle), and aspect ratio (right) for WT, ErbB2^{amp,} and PI3K^{H1047R} expressing cells (n > 30 cells for N = 4 biological replicates). (F) Scratch wound closure kinetics and (G) final closure percentage for monolayers of WT or mutant-expressing cells (N = 4 biological replicates). (H) RT-qPCR of EMT transcription factor expression in each cell line, normalized to the expression in WT MCF10A (N = 3 biological replicates). (I) Fraction of proliferating cells as measured by 24 h Edu assay (average of n = 3 images from each of N = 5 biological replicates). (J) mRNA expression data for tumors collected in METABRIC study, demonstrating expression levels of ZEB1 (left), CDH1 (middle), and MKI67 (right) in ErbB2^{amp}- and PI3K^{H1047R}-expressing tumors. Student's t-test or ANOVA with Bonferroni post hoc testing used where appropriate. All error bars indicate standard error. Q-values noted where appropriate. * $p \leq 0.05$; ** $p \leq 0.01$, ***$p \leq 0.001$.

crucial processes, it has become clear that temporal encoding is a means by which different ligands and environmental contexts can drive distinct cellular responses using common intracellular hardware.

In cancer, somatic mutations rewire intracellular pathways, fundamentally altering cellular behavior in a manner that confers a selective advantage to the cells harboring the change. These advantages, commonly known as the "hallmarks of malignancy," are behavioral changes, including increased proliferation, invasion or overall survival, that permit expansion of the transformed population of cells.[12−14] However, the link between a specific signaling change and the resultant cellular phenotype is not always directly apparent. These associations have been further complicated by emerging evidence which suggests that mutations affecting the same signaling pathway can drive distinct cellular responses.[15−17] Given the role of signal dynamics in homeostasis, it stands to reason that altered signaling dynamics could contribute to carcinogenesis as well. Recent work has demonstrated that cells harboring the BRAF G469A mutation, a known oncogenic mutation in lung cancer, show slower decay of Erk signaling; thus, in these cells, high-frequency signals result in sustained Erk signals, which ultimately drives increased cellular proliferation in response to an otherwise benign stimulus.[18] While increased proliferation is only an element of carcinogenesis, this work illustrates how oncogenic mutations can alter signaling dynamics in a

https://doi.org/10.1021/acssynbio.5c00651
ACS Synth. Biol. XXXX, XXX, XXX−XXX

manner that confers selective advantages to cells harboring these mutations.

Much like the MAPK axis, the PI3K-Akt signaling axis, a key regulator of proliferation, survival, migration, and metabolism, is increasingly recognized to operate under dynamic control.[19−21] Early work on insulin signaling demonstrated that both the magnitude and duration of PI3K activity are critical for glucose homeostasis,[22−24] and subsequent studies have supported a broader role for PI3K dynamics in controlling cellular function.[25−28] Given that PI3K dysfunction has been found in over 50% of all cancers, and in more than 70% of breast cancers, it is critical to understand whether oncogenic mutations within this axis reshape PI3K signaling dynamics in a mutation-specific manner.[29−31]

Our recent work developing a mammary-duct-on-a-chip demonstrated that the *ErbB2* amplification and the *PIK3CA*^{H1047R} mutation—both of which enhance PI3K-Akt signaling—lead to distinct cellular behaviors *in vitro*, a behavior consistent with clinical findings suggesting that these mutations define distinct molecular subtypes of breast cancer with different prognoses.[30,32−37] We hypothesized that these phenotypic differences might emerge from mutation-specific modulation of the dynamics of PI3K-Akt signaling.

Here, we demonstrate that each mutation produces a unique dynamic response to EGF stimulation, reflecting distinct, mutation-specific rewiring of the PI3K-Akt pathway. To test the role of these altered signaling dynamics in the observed phenotypes, we constructed and applied an optogenetically controlled PI3K module (OptoPI3K) to engineer a mammary epithelial cell line in which we have direct, programmable and high-fidelity control over intracellular PI3K signaling patterns. Using this system, we were able to deliver mutant-specific PI3K dynamics to these nontransformed cells. We found that these rewired dynamics were sufficient to recapitulate some key features of the cancer-associated mutant phenotypes, including regulation of epithelial-to-mesenchymal transition. These data suggest that temporal encoding of PI3K-Akt signaling, rather than simple binary activation, contributes to some oncogenic changes observed and demonstrates the power of modular optogenetic tools to dissect, rewire, and ultimately reprogram native signaling networks in living cells.

RESULTS

ErbB2*amp* and the PI3K H1047R Mutation Drive Distinct Cellular Responses in MCF10A Mammary Epithelium

We have previously shown that MCF10A mammary epithelial cells harboring the *ErbB2* amplification (herein referred to "ErbB2^{amp}") or the *PIK3CA H1047R* mutation (herein referred to as "PI3K^{H1047R}")—common breast cancer mutations with divergent prognoses—show distinct phenotypes when cultured in a bioengineered mammary duct-on-a-chip, despite both driving significant activation of the PI3K-Akt signaling axis.[32] To investigate the mechanisms by which these two mutations drive differential changes in cell behavior, we utilized a nontumorigenic mammary epithelial cell line, MCF10A, which does not natively harbor PI3K mutations or *ErbB2* amplifications. The wild-type (WT) MCF10A cell line was modified with a doxycycline-inducible expression system, such that either oncogene would be transiently expressed following doxycycline stimulation. This facilitates comparison of the consequences of each mutation shortly after expression, while controlling for the duration of altered signaling to minimize the accumulation of off-target effects that can result from prolonged oncogene exposure (Figure 1A).[38]

To assess the morphological consequences of each mutation on gross mammary duct morphology, cells were induced with doxycycline (1 μg/mL) 3 days prior to seeding into our 3D engineered mammary duct platform, which were then cultured for 5 days before morphological characterization was performed. While mammary ducts seeded with WT MCF10A cells formed a peripheral monolayer around a central lumen with no clear evidence of invasion, cells expressing either mutation showed distinct morphologic and invasive patterns (Figure 1B). Ducts seeded with ErbB2^{amp} cells showed hypercellularity, with proliferation overtaking the monolayer lining, and filling of the central lumen of the duct. Invasion, while rare in these ducts, proceeded in a multicellular manner. In contrast, ducts seeded with PI3K^{H1047R} expressing cells showed disruption of the monolayer, with cells invading into the surrounding matrix as single cells and significantly more sprouts per duct than the ErbB2^{amp} or WT condition (Figure 1C). These findings agree with our previous results using cell lines permanently expressing these oncogenes, suggesting that even short durations of oncogene expression are sufficient to drive the mutation-specific responses.[32]

To examine mutation-specific morphological changes in a more quantitative manner, we next characterized the morphology of each mutant cell line in 2D. While WT and ErbB2^{amp} cells showed a traditional cobblestone epithelial phenotype and were indistinguishable from each other in terms of cell area, aspect ratio and circularity, cells expressing the PI3K^{H1047R} mutation displayed an enlarged, highly elongated phenotype, consistent with their 3D morphology (Figure 1D,E). Given that cells harboring the PI3K^{H1047R} mutation showed an invasive phenotype in our 3D model, we next assessed cellular motility in 2D to investigate if the increased invasion was a result of increased migratory ability. Comparison of closure rates in a 2D scratch wound assay demonstrated that cells harboring the PI3K^{H1047R} mutation closed the wound significantly faster than cells harboring ErbB2^{amp} or WT cells (Figure 1F,G). Time lapse imaging also demonstrated that epithelial cells with the PI3K mutation tended to migrate as single cells across the wound margin, while WT MCF10A and MCF10A harboring the *ErbB2* amplification tended to move as a collective monolayer across the wound margin, suggesting differences in intercellular adhesions in each cell line.

The increased migratory behavior, single-cell migratory trajectory, and elongated morphology seen in the PI3K^{H1047R} cells were all consistent with an epithelial to mesenchymal transformation (EMT) in these cells.[39,40] As a positive control for EMT behavior, WT MCF10A were stimulated with TGF-β, a known inducer of EMT, in each of the preceding assays.[41] WT MCF10A cells stimulated with TGF-β showed increased cell area, aspect ratio and migratory rate, results consistent with the morphologic and behavioral changes observed in the PI3K^{H1047R} mutants, suggesting that the PI3K H1047R mutation drives an EMT-like phenotype in MCF10A (Supplemental Figure 1A,B). To further characterize this EMT, the expression of transcriptional regulators associated with EMT were quantified in each mutant cell line using RT-qPCR. While both PI3K^{H1047R} and TGF-β treated MCF10A cells showed a significant increase in the expression of several EMT transcription factors, ErbB2^{amp} and WT MCF10A showed no significant expression of these factors, further

https://doi.org/10.1021/acssynbio.5c00651
ACS Synth. Biol. XXXX, XXX, XXX−XXX

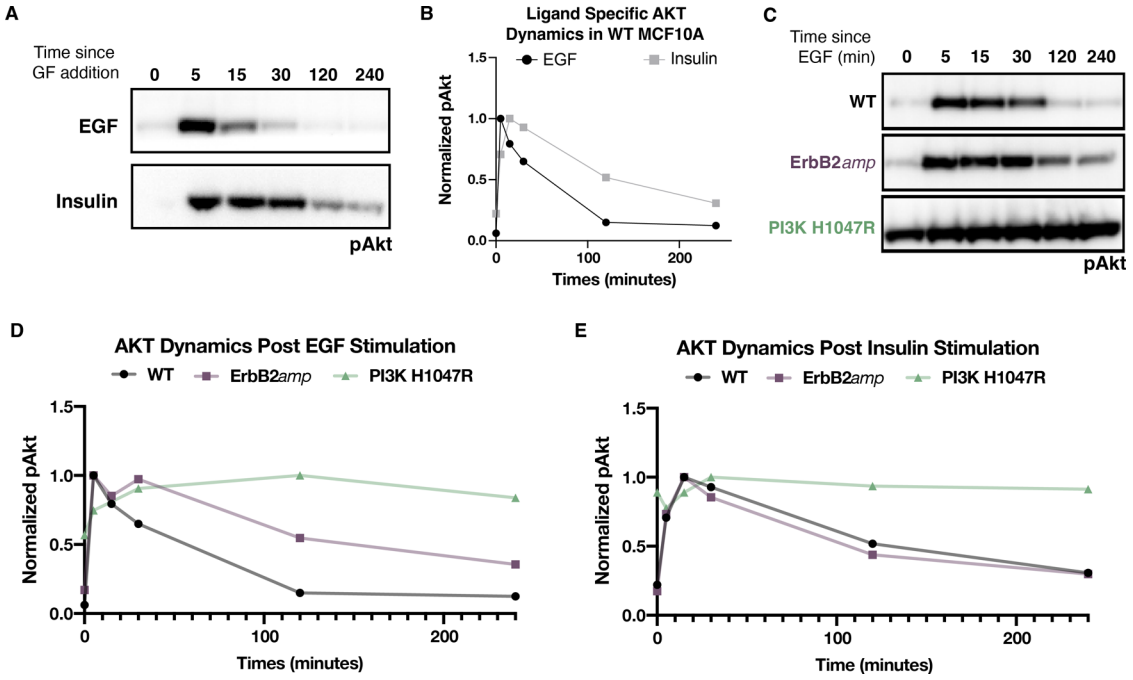

Figure 2. Distinct PI3K axis mutations differentially rewire PI3K-Akt axis signal transduction. (A) Time course of PI3K activity in serum-starved MCF10A cells in response to EGF (5 ng/mL) or insulin (100 μg/mL) stimulation, as measured by pAkt levels. (B) Quantification of pAkt levels in WT MCF10A treated with EGF or insulin, normalized to the maximal value. (C) Representative Western blot demonstrating prolongation of pAkt activation in response to ErbB2 overexpression and constitutive pAkt activation in PI3K^{H1047R}-expressing cells. (D,E) Time course of pAkt levels in PI3K^{H1047R} and ErbB2^{amp} cells stimulated with EGF (D) and insulin (E), again normalized to peak value.

suggesting that cells harboring the PI3K^{H1047R} mutation undergo some degree of EMT as a result of this genomic insult (Figure 1H, Supplementary Figure 1C).

In contrast to the highly invasive PI3K^{H1047R} cells, ErbB2^{amp} cells cultured within our engineered mammary duct showed a high degree of ductal infilling (Figure 1B), suggesting that this genomic insult might drive a more proliferative response. This hypothesis was confirmed using a 2D EdU assay, which demonstrated that ErbB2^{amp} cells were significantly more proliferative than WT or PI3K^{H1047R} cells (Figure 1I).

To validate that these in vitro findings correlate with the clinical behavior of tumors harboring these mutations *in vivo*, we analyzed mRNA expression of patient breast tumors collected from patients as part of the METABRIC study, using gene expression of key markers as a surrogate for clinical behavior. This analysis demonstrated that breast tumors harboring the PI3K^{H1047R} mutation had significantly increased expression of the EMT transcriptional regulator *ZEB1*, in alignment with the results in Figure 1H, as well as decreased expression of *CDH1* (E-cadherin), suggesting some loss of epithelial character and a degree of EMT (Figure 1J, left, middle).[36,37] In contrast, patients with tumors harboring the *Erb*B2 amplification had significantly increased expression of *MKI67*, a marker of proliferation, when compared to tumors harboring the PI3K^{H1047R} mutation, correlating with the increased proliferation we observed in the 2D assay (Figure 1J, right). Collectively, these results establish a dichotomy in behavioral consequences downstream of these two common PI3K axis lesions: MCF10A harboring the PI3K^{H1047R} mutation undergo EMT without significant proliferation, while ErbB2^{amp} MCF10A show no significant EMT but rather a hyperproliferative phenotype.

Distinct PI3K Axis Mutations Differentially Rewire PI3K-Akt Axis Signal Transduction

We next sought to uncover the origin of the mutation-specific differences in cell behavior observed. While both mutations are known to increase the amount of PI3K-Akt axis activation,[42] we hypothesized that they might differentially modulate PI3K signaling dynamics, and that this rewiring might underscore the observed phenotypic differences. Given that the PIK3CA^{H1047R} mutation is a constitutively activating mutation, we expected sustained PI3K-Akt activity even in the absence of external stimuli.[43] In contrast, ErbB2^{amp} increases overall receptor expression, but the ErbB2-containing complexes remain subject to endogenous regulatory mechanisms, albeit with a slower rate of signal termination due to the increased prevalence of ErbB2 monomers available for complex formation.[35] Based on these mechanistic differences, we hypothesized that the temporal profile of PI3K-Akt activity in response to stimulation would differ between the two mutations.

Two components of the MCF10A medium, EGF and insulin, are known PI3K-Akt axis agonists which have been shown to drive distinct activation patterns of PI3K-Akt signaling in HeLa cells.[27] To quantify response to each, serum starved WT MCF10A were stimulated with either ligand and the resultant pathway activation measured over time. These experiments show that EGF stimulation induces a rapid, transient spike in PI3K activity with a half-life of approximately 30 min, whereas insulin stimulation drives a prolonged activation, confirming that, like HeLa cells, MCF10A cells can encode different stimuli through distinct PI3K-Akt signaling dynamics (Figure 2A,B). We next quantified ligand-stimulated PI3K-Akt signaling in cells harboring each mutation. In contrast to WT cells, ErbB2^{amp} cells showed a

https://doi.org/10.1021/acssynbio.5c00651
ACS Synth. Biol. XXXX, XXX, XXX−XXX

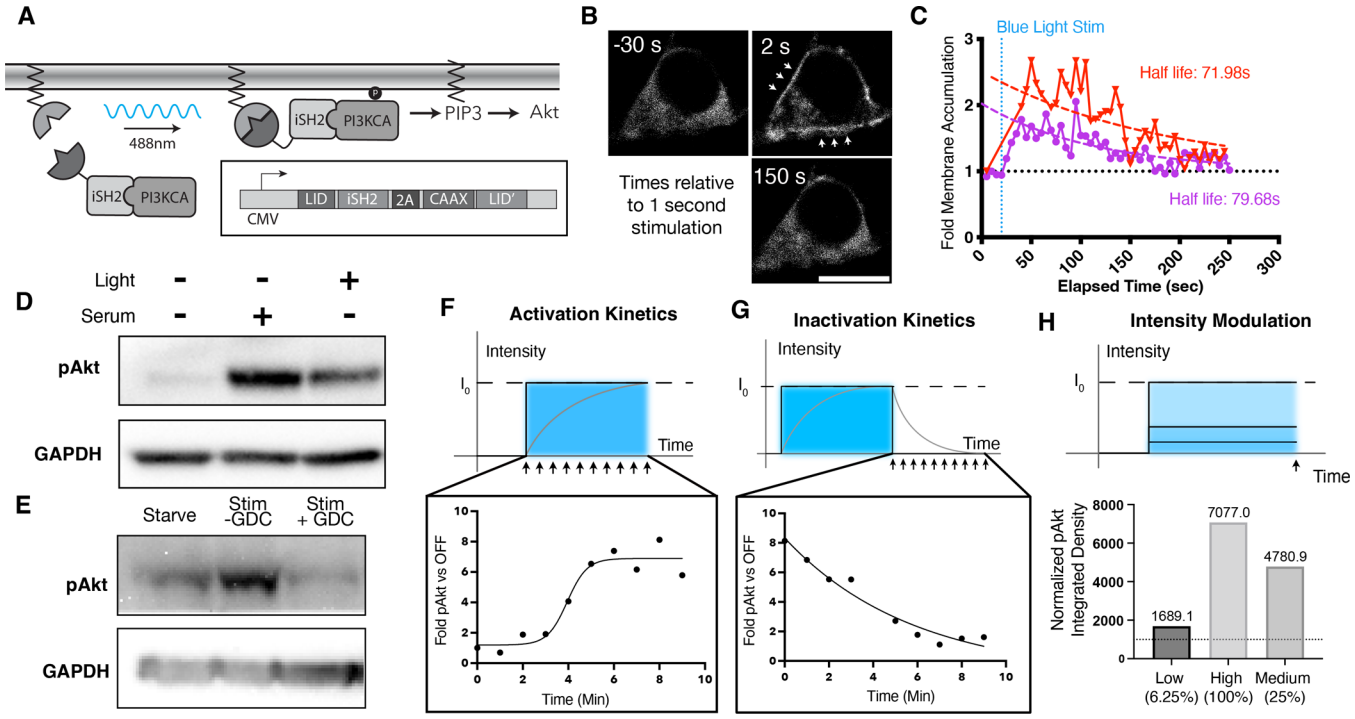

Figure 3. OptoPI3K enables rapid, orthogonal light-dependent actuation of PI3K signaling. (a) Schematic of the OptoPI3K system. An iLID-nano domain is constitutively tethered to the cell membrane and a soluble ssPb domain is tethered to an iSH2 domain. Following blue light exposure, the two domains come together, bringing PI3K to the membrane and driving downstream signaling. (B) HEK293FT cells expressing the OptoPI3K system with an additional mCherry-tagged iSH2 domain to explore translocation dynamics shows membrane accumulation in response to light (scale bar = 10 μm). Arrows highlighting membrane accumulation. (C) Quantification of membrane accumulation in response to stimulus. Lines indicate individual cells following stimulation. Dashed lines are exponential decay fit for half-life measurement. (D) MCF10A cells expressing the OptoPI3K system show activation of Akt in response to light with a similar magnitude to stimulation with serum. (E) GDC-0941 pretreatment of cells abrogates downstream response to blue light stimulation. (F) Activation of OptoPI3K in response to light stimulation. Note that top panel shows stimulation pattern, while bottom panel demonstrates measured pAkt levels (G). Inactivation kinetics following the removal of a 10 min blue light stimulus. (H) Modulating stimulus intensity drives differential levels of PI3K activation within the cell in a nonlinear fashion.

prolonged response to EGF stimulation, with a half-life of approximately 120 min. As expected, $PI3K^{H1047R}$ expressing mutants showed constitutive EGF-independent PI3K activation (Figure 2C,D).

To confirm that the prolongation of PI3K-Akt signaling in $ErbB2^{amp}$ cells was directly the result of the increased EGF-family receptor expression, cells were stimulated with insulin, an agonist that signals independently of the ErbB2 signaling complex. In this context, both the WT and $ErbB2^{amp}$ cells showed a similar pAkt temporal response, suggesting that the prolonged axis activation in EGF-stimulated $ErbB2^{amp}$ cells was due to ErbB2-driven signaling rather than a global alteration in PI3K-Akt signaling within the cell (Figure 2E).

Collectively, these findings suggest that MCF10A cells can encode ligand identity into PI3K axis signaling dynamics and that oncogenic mutations affecting this axis can reshape the dynamic response to stimulation. We next investigated whether these differences in signaling dynamics could drive the distinct phenotypes observed in mutant cells.

OptoPI3K Enables Rapid, Orthogonal Light-Dependent Actuation of PI3K Signaling

To explore the role of mutant-specific rewiring of PI3K signaling in the pathogenesis of each mutation, we set out to develop an approach to directly (orthogonally) control PI3K signaling dynamics within the cell. To this end, we developed an optogenetic construct, OptoPI3K, which permits direct control over the activation of intracellular PI3K signaling. Inspired by designs of other recently developed optogenetic controlled PI3K modules,[44−47] OptoPI3K relies on inducible localization of the PI3K p110α subunit to the cellular membrane, where it can convert PIP_2 to PIP_3 to activate downstream signaling. To achieve this, we capitalized on the rapid ON/OFF kinetics afforded by the iLID system of light-inducible dimers to enable high fidelity intracellular reconstitution of an incident blue light stimulus.[48,49] Using this construct, we targeted the iLID-nano domain to the membrane via a CAAX motif, and fused the complementary ssPb fragment to an inter-SH2 (iSH2) domain, a naturally occurring p110α binding domain that lacks substantial inhibitory activity and has proven efficacious in previously reported PI3K inducible dimerization systems (Figure 3A).[44,47,50,51]

To confirm membrane recruitment in response to blue light, an mCherry fluorescent tag was added to the iSH2 fragment to enable visualization of its intracellular position. Upon blue light stimulation, there was a clear and rapid translocation of the iSH2 domain from the cytosol to the membrane, consistent with membrane localization of the soluble fragment. When the stimulus was removed, a fast dissociation from the membrane was recorded, with an average dissociation half-life of 76.3 s (n = 2), consistent with previously reported iLID dimerization/dissociation kinetics (Figure 3B,C).[48] Collectively, these results suggest that incorporation of the iLID system into the OptoPI3K construct does not affect its rapid ON/OFF kinetics, consistent with previously published work.[44−46]

https://doi.org/10.1021/acssynbio.5c00651
ACS Synth. Biol. XXXX, XXX, XXX−XXX

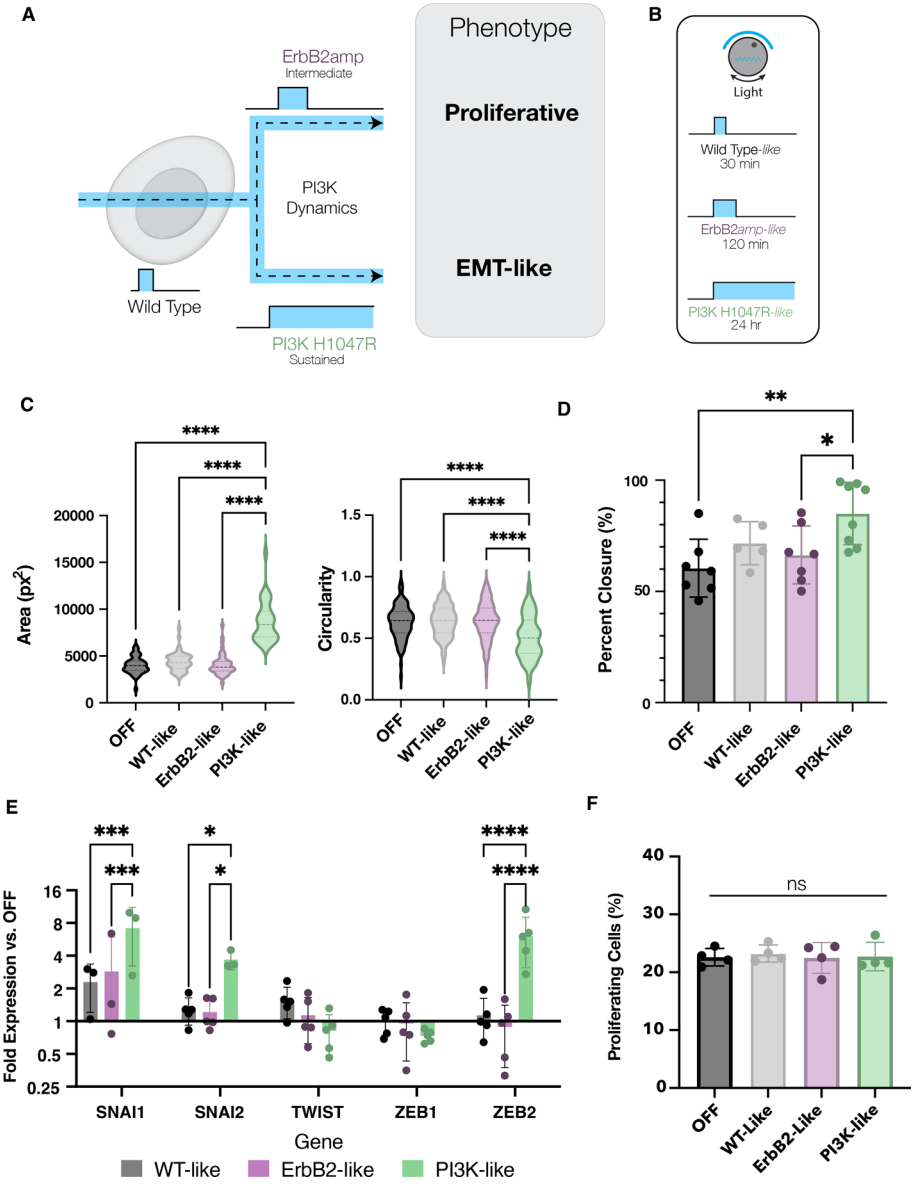

Figure 4. Altered PI3K dynamics contribute to the development of some of the observed mutation-specific phenotypes. (A) Schematic summarizing hypothesis relating mutation-specific rewiring of PI3K dynamics to cellular phenotype. (B) Definition of signaling for WT-like, ErbB2^{amp}-like, and PI3K^{H1047R}-like signaling. For the sake of readability, ErbB2^{amp}-like has been shortened to "ErbB2-like", and PI3K^{H1047R}-like has been shorted to "PI3K-like" within the figure (C) Area and circularity measurements of MCF10A monolayers exposed to each light signal. (D) Delivery of a PI3K^{H1047R}-like signal to OptoPI3K-expressing MCF10A drove a significant increase in wound closure as compared to WT-like PI3K signal or the ErbB2^{amp}-like signal. (E) Expression of EMT transcription factors in OptoPI3K-expressing cells stimulated with each mutant-specific signal, normalized to cells exposed to no light. (F) Fraction of cells with Edu incorporation after exposure to each of the mutant-specific PI3K signals. All error bars indicate the standard error. *$p \leq 0.05$; **$p \leq 0.01$, ***$p \leq 0.001$.

We next tested the functional activity of the OptoPI3K system. Serum-starved MCF10A cells were stimulated with blue light and the resultant axis activation was measured via quantification of pAkt levels. While starved cells showed minimal Akt activation, both the serum stimulated (positive control) and blue-light treated cells showed robust pAkt accumulation, demonstrating light-dependent activation of PI3K-Akt signaling within the cell (Figure 3D). This effect was abrogated by the pan-PI3K inhibitor GDC-0941, demonstrating that this light-induced increase in signaling is mediated via endogenous PI3K (Figure 3E).

To evaluate the kinetics of the optoPI3K system, we performed serial Western blotting following blue light stimulation. All stimulation experiments were performed using a custom, Arduino-based blue-light stimulation system that enables control over duration and intensity of stimulation within each well of a 24 well plate. Stimulation of cells expressing this construct showed a >4-fold increase in pAkt within 4 min of stimulation, peaking at an 8-fold increase within 6 min (Figure 3F). Upon removal of the light stimulus, pAkt levels rapidly returned to baseline with a decay half-life of ~3−4 min and full deactivation within 7 min (Figure 3G). Finally, we tested OptoPI3K's response to light intensity modulation. Cells were stimulated for 30 min with varying light intensities (6.25, 25, and 100% of maximal LED output), which resulted in graded, though nonlinear, increases in pAkt with higher intensities (Figure 3H). Importantly, 24 h continuous stimulation at maximal intensity did not affect

https://doi.org/10.1021/acssynbio.5c00651
ACS Synth. Biol. XXXX, XXX, XXX−XXX

cell viability, as assessed by both cell counts and MTT assays (Supplemental Figure 2). Collectively, these results demonstrate that OptoPI3K enables precise, user-programmable control over PI3K signaling with high temporal fidelity, facilitating our efforts to dissect the role of PI3K dynamics in cellular decision making and behavior.

Altered PI3K Dynamics Contribute to the Development of Some of the Observed Mutation-Specific Phenotypes

To investigate whether the measured mutation-specific changes to PI3K dynamics contribute to the distinct phenotypes observed in each mutant, we used OptoPI3K to mimic the mutation-specific signaling patterns in nontransformed MCF10A cells using programmed light inputs. Cells were stimulated with PI3K patterns analogous to those recorded in Figure 2, including a short, "WT-like" stimulus, an intermediate-length stimulus resembling that of ErbB2^{amp} cells ("ErbB2^{amp}-like" stimulus) and a sustained signal mimicking *PIK3CA*^{H1047R} mutants ("PI3K^{H1047R}-like" stimulus) (Figure 4A,B). Given the results of the mutation-specific phenotypes previously observed, we hypothesized that the ErbB2^{amp}-like stimulus would promote proliferation, while the PI3K^{H1047R}-like stimulus would induce an EMT-like phenotype.

Using the same metrics as described in Figure 1, we first explored the morphological response to the distinct PI3K signals. While all cells started off with the WT cobblestone morphology, cells exposed to the PIK3CA^{H1047R}-like signal showed an increase in cell size and decrease in cell circularity in response to stimulation, a result consistent with the morphological changes seen in the PI3K^{H1047R} mutants and those with TGF-β driven EMT (Figure 4C, Supplemental Figure 1). Similarly, despite an identical population of original cells, the PI3K^{H1047R}-like signal drove a significantly increased wound closure in the scratch wound assays compared to the WT or ErbB2^{amp}-like patterns of stimulation, further supporting the link between sustained PI3K exposure, increased motility, and EMT-like behavior (Figure 4D, Supplemental Figure 3). Next, we evaluated the role of PI3K signal duration on the expression of EMT transcriptional regulators. Cells exposed to the PI3K^{H1047R}-like signal had significantly increased expression of *SNAI1*, *SNAI2*, and *ZEB2*, while cells exposed to the ErbB2^{amp}-like or WT-like stimulation of cells did not (Figure 4E). These results mirror the mutation-specific increase in EMT transcriptional regulators reported in Figure 1, suggesting that sustained PI3K activity contributes to EMT changes observed in PI3K^{H1047R} mutants.

Finally, we examined the role of PI3K signaling dynamics in ErbB2^{amp}-mediated proliferation. Using an Edu proliferation assay, MCF10A were stimulated with each pattern of light stimulus and the fraction of cells entering cell cycle was quantified (Figure 4F). Surprisingly, none of the PI3K stimulation patterns significantly increased proliferation, despite our previous observation of enhanced proliferation in ErbB2^{amp} cells, suggesting that ErbB2^{amp}-driven proliferation requires additional signaling inputs beyond PI3K duration alone. Overall, these results demonstrate that sustained PI3K stimulation is sufficient to induce an EMT-like response in MCF10A cells. However, intermediate duration PI3K activation alone is insufficient to drive significant proliferation, indicating that the observed ErbB2^{amp}-mediated proliferative response may involve additional, PI3K-independent mechanisms.

DISCUSSION

In this work, we demonstrate that activating mutations targeting the PI3K-Akt signaling axis can drive distinct behavioral changes in cells harboring these mutations. Specifically, *ErbB2* amplification promotes a proliferative phenotype, whereas the PIK3CA^{H1047R} mutation drives an EMT-like transformation in MCF10A mammary epithelial cells. Observing that these mutations differentially modulated PI3K signaling dynamics, we hypothesized that these altered dynamics might contribute to the distinct responses seen. To test this, we applied the established power of optogenetics and developed a light inducible PI3K enzyme to directly control the dynamics of endogenous PI3K signaling in nontransformed cells.[44−47,52,53] Using this tool, we showed that sustained PI3K activation is sufficient to drive the observed EMT-like changes observed in PIK3CA^{H1047R}, while introducing an ErbB2^{amp}-like pattern of PI3K signaling was insufficient to replicate the proliferative burst observed in *ErbB2*-amplified cells.

These results support the emerging paradigm that different oncogenic mutations within a shared signaling pathway can produce distinct cellular outcomes. Prior studies have shown that *PIK3CA* and *Akt* mutations can confer unique responses to mTOR inhibition and even promote distinct cellular behaviors, despite grossly enhancing PI3K-Akt activity.[54−56] Even subtle genetic variations, such as SNPs affecting single amino acid residues can drive divergent cellular responses.[57] Our findings demonstrating the importance of PI3K signaling dynamics in some of the oncogenic phenotypes suggest that additional study of this pathway may be warranted.

The development of tools to enable precise, orthogonal modulation of critical signaling pathways has gained recent traction. Several chemical induced dimerization systems to toggle PI3K-Akt activity have been previously described, including some systems that permit spatiotemporal localization within the cell.[58,59] While these systems have facilitated significant advances in our understanding of how PI3K signaling contributes to migration and metabolism, chemical dimerization systems are often limited by relatively slow off kinetics, do not easily permit spatial localization of activation, and their ligands can sometimes generate off-target signaling effects within the cell, all of which limit their ability to replicate complex oncogene-associated changes in signaling dynamics.[60] In recent years, optogenetics has emerged as an alternative platform by which cellular signaling can be orthogonally manipulated, with new tools emerging regularly that permit the orthogonal control of Erk, p53, NF-κB, YAP and even PI3K, among others.[18,46,47,53,61−65] These constructs have revolutionized the field, as they enable activation of cellular signaling in response to incident light, which can be easily manipulated using inexpensive LEDs and benchtop microcontrollers. Furthermore, many of these tools do not require lengthy wash-out periods for the cessation of signaling, enabling higher-fidelity replication of incident stimulus than could be achieved with the older chemical dimerization systems. For these reasons, these systems have readily emerged as powerful tools to investigate the role of signaling dynamics.[66] Indeed, our study builds on extensive prior work developing and applying optogenetic tools (including light-induced PI3K modules) to interrogate the role of signaling dynamics in insulin regulation, drug resistance, protein trafficking and cell migration, among other areas of focus.[44−47,52,53,63]

https://doi.org/10.1021/acssynbio.5c00651
ACS Synth. Biol. XXXX, XXX, XXX−XXX

Building off these developments, we describe a light-inducible PI3K system that enables the rapid and orthogonal activation of PI3K signaling in cells, enabling deeper investigation into how the mutation-specific changes to signaling dynamics drive the observed behavioral responses. Previous work has established that constitutive PI3K signaling can drive an EMT-like change in cellular phenotype, though these studies were conducted in a tumorigenic background.[67−70] Here, we confirm that sustained PI3K activation is sufficient to drive EMT-like changes in a nontumorigenic context, independent of specific oncogenic mutations. This suggests that signal duration, rather than mutation-specific interactions, is a key determinant of PI3K-mediated EMT.

Intriguingly, new evidence suggests that the *PIK3CA H1047R* mutation is not a simple pan-PI3K activator, as it has conventionally been considered, but rather a dose- and context-dependent modulator of growth factor signaling.[71] While we observed constitutive activation in the setting of the H1047R mutation, this could potentially be explained by bulk population-level measurements and overexpression of the mutant PIK3CA H1047R protein used in our study, which are distinct from the precise allelic manipulation and single-cell readouts employed in the recently reported study.[71] While the work further supports the role of temporal dynamics in PI3K-mediated effects, it suggests additional studies focused on emulating the more complex layers of PI3K signaling are warranted. Indeed, the current study focused solely on the altered duration of signaling. Other aspects of signaling dynamics—including the role of signaling intensity, persistence, oscillations, and basal activity—could be investigated in future work with optogenetic tools, which may provide deeper insights into how signaling impacts downstream responses. In addition to temporal control, these inducible systems could also open the door to studying the effects of mutation-induced signaling strength/dose by titrating levels of expression of the activated constructs. For example, future studies could clarify whether the amount of mutated PI3K H1047R or ErbB2 expressed impacts either dynamics or strength of downstream PI3K signaling, and subsequent cellular phenotype. A more complete systems understanding of this pathway could help shed light on how specific mutations in pathway members or amplification copy numbers exist in the broader landscape of aberrant PI3K-drivenoncogenesis.

Clinically, our findings provide an intriguing perspective on the differential aggressiveness of *ErbB2*-amplified and *PIK3CA* mutant breast cancers. While patients with *ErbB2*-amplified tumors exhibit increased mortality compared to those with the *PIK3CA H1047R* mutation, our data suggest the *PIK3CA* mutation drives a more invasive, mesenchymal-like phenotype, while the *ErbB2* amplification promotes a more localized, proliferative response. As metastasis is often considered to be the major driver of cancer mortality, the clinical data and *in vitro* data presented here seem discordant.[72] This discrepancy raises the interesting possibility that the PI3K mutation may induce a "locked-in" mesenchymal state. Pathologically, metastatic dissemination requires that circulating cells undergo the reverse of EMT, a process known as mesenchymal-to-epithelial transition (MET), to engraft and establish secondary tumors. If sustained PI3K signaling "locks" cells into a mesenchymal state, functionally impairing MET, this would ultimately reduce metastatic burden by prohibiting establishment of secondary tumors, counterbalancing the increasingly invasive phenotype. Intriguingly, a recent study shows that coexpression of the *PIK3CA H1047R* mutation in an *in vivo* model of *ErbB2*-amplified cancer significantly decreases metastatic burden, an observation consistent with this paradigm of sustained PI3K activity "locking-in" the mesenchymal state.[73] While PI3K inhibitors have shown limited clinical efficacy, our findings raise the provocative question of whether PI3K *agonism* could be therapeutically leveraged to reduce metastatic spread by enforcing a mesenchymal state.

Despite these insights, several limitations remain. Our analyses of PI3K dynamics relied on Western blotting, which is a population level measurement that averages a large number of cellular responses into a single data point, missing discrete differences in individual dynamics.[74] Efforts are underway to implement real-time Akt biosensors to further explore the role of PI3K dynamics in breast cancer progression at the single-cell level, which could provide a more granular view of how signaling dynamics shape phenotypic outcomes. Additionally, despite the promise of our OptoPI3K system in investigating cancer-associated signaling dynamics, there are important limitations of this tool and study. Though our data shows relatively low levels of basal activation (Figure 3D), this was achieved through careful attention to light shielding, in both shared incubator and culture hoods. Furthermore, most experiments were performed with freshly thawed cell lines, as we noted that experimental variability increased significantly with passaging beyond 2−3 times − likely due to a combination of cells selecting against the construct, as well as some basal leak in uninduced cells leading to corruption of the WT state. Despite these limitations, the ability to orthogonally control intracellular PI3K signaling permits deeper exploration into the mechanisms by which PI3K-mediated oncogenesis occurs and may one day elucidate novel strategies by which we could precisely target individual mutations to halt tumor progression.

CONCLUSIONS

In this study, we demonstrate that two commonly occurring mutations in breast cancer—*ErbB2* amplification and the *PIK3CA H1047R* mutation—drive distinct phenotypic outcomes in mammary epithelial cells, despite converging on the same PI3K-Akt signaling axis. We show that these genomic alterations differentially reshape signal transduction within the PI3K axis, and leveraging an optogenetic toolkit to precisely control PI3K activity in nontumorigenic cells, we find that sustained PI3K activation is sufficient to drive the EMT-like behavior observed in *PIK3CA* mutant cells. In contrast, the prolonged PI3K activation associated with *ErbB2* amplification fails to recapitulate the proliferative burst observed in *ErbB2*-amplified cells, suggesting that additional signaling inputs are required for this response. Together, these findings emphasize the importance of signaling dynamics, rather than binary pathway activation, in shaping oncogenic phenotypes, and highlight how new synthetic signaling tools are needed to further elucidate how distinct mutations within the same signaling network can produce divergent cellular outcomes. These insights have significant implications for understanding cancer progression and for the development of novel approaches to shed light on the underlying signaling mechanisms that drive it.

https://doi.org/10.1021/acssynbio.5c00651
ACS Synth. Biol. XXXX, XXX, XXX−XXX

METHODS

Cell Culture

MCF10A human mammary epithelial cells (ATCC) were cultured in growth medium consisting of DMEM/F12 (1:1 Gibco) supplemented with 5% horse serum (Invitrogen), 20 ng/mL EGF (Peprotech), 0.5 mg/mL hydrocortisone (Sigma), 100 ng/mL cholera toxin (Sigma), 10 μg/mL insulin (Sigma) and 1% penicillin/streptomycin (Invitrogen), as described previously.[75] When used in 2D or 3D culture assays, MCF10A cells were transitioned to "Assay" medium, consisting of phenol red free DMEM/F12 (1:1 Gibco) supplemented with 2% horse serum (Invitrogen), 5 ng/mL EGF (Peprotech), 0.5 mg/mL hydrocortisone (Sigma), 100 ng/mL cholera toxin (Sigma), 10 ug/mL insulin (Sigma) and 1% penicillin/streptomycin (Invitrogen). For starvation experiments (all growth factor stimulation experiments), cells were cultured in "Starvation Medium", consisting of phenol red free DMEM/F12 (1:1 Gibco) supplemented with 0.5 mg/mL hydrocortisone (Sigma), 100 ng/mL cholera toxin (Sigma), and 1% pen/strep (Invitrogen).[76] HEK293FT cells (Thermo Fisher Scientific R700-07) were grown in high-glucose DMEM supplemented with 10% fetal bovine serum (Sigma), 1% penicillin/streptomycin (Invitrogen). All cells were cultured at 5% CO_2 and 37 °C in a humidified incubator. Doxycycline (Thermo Fisher Scientific) for induction was used at 1000 ng/mL, unless otherwise specified.

Cloning and Retroviral Infection

To synthesize the inducible oncogene cassettes, pCW57-MCS1-2A-MCS2 (Addgene plasmid #71782) was digested with the restriction endonucleases *NheI* and *Sal*I. mCherry was inserted into the split fragment at the first MCS via Gibson Assembly. The resultant plasmid was then split at MCS2 using the restriction enzymes *MluI* and *Bam*HI. *HER2/Erb* (Addgene plasmid #40978) or *PIK3CA(H1047R)* (Addgene plasmid #12524) were inserted into the cut site via Gibson Assembly.

To construct OptoPI3K, the ssPb domain from the plasmid PLL7.0: tgRFPt-SSPB WT (Addgene Plasmid #60415) was placed C-terminally to the iSH2 domain in the plasmid mCherry-CRY2-iSH2 (Addgene Plasmid #66839) via Gibson assembly. The iSH2-SSPB fragment was then PCR'd off the resultant construct and inserted into a pLenti-CMV-GFP-Puro (Addgene Plasmid #17447) using Gibson Assembly. The stock iLID-CAAX construct (Addgene Plasmid #85680) was also inserted into the pLenti CMB construct via Gibson Assembly. For localization experiments, mCherry was added N-terminally to the OptoPI3K construct via Gibson Assembly using the mCherry from the original Addgene plasmid #66839.

Lentiviral packaging was performed by plating 500,000 HEK293FT cells into a 6 well plate. 24 h later, 1 μg of the lentiviral donor plasmid, 700 ng of pCMVR8.74 (Addgene plasmid #22036), 200 ng of pMD2.G VSVG (Addgene plasmid #12259) and 100 ng of pAdVantage (Promega) were cotransfected into each well using a NaCL-polyethylenimine (PEI, 7.5 mM linear PEI stock, nitrogen/phosphorus ratio of 20, Polysciences) transfection. Following transfection, cells were incubated for 72 h prior to supernatant harvesting, concentrated using the PEG-IT viral precipitating agent (SBI) and resuspended in PBS. These viral particles were then added to MCF10A cells and incubated overnight. 48 h after viral transduction, cells were exposed to 2 μg puromycin for 2 days. Lines were immediately tested for expression via Western blot or fluorescence microscopy and successful lines were cryopreserved immediately.

Mammary Duct-on-a-Chip Fabrication and Seeding

Devices were fabricated as previously described.[32] Briefly, polydimethylsiloxane (PDMS, Sylgard 184, Dow-Corning) was mixed in a 10:1 ratio with its curing agent and poured over a microfabricated mold. PDMS was allowed to polymerize at 60 °C overnight before it was removed from its silicon wafer. Media holes were punched using a 5 mm biopsy punch, while collagen ports were punched using a 2 mm biopsy punch. Devices were cut into individual devices, treated with plasma for 1 min and adhered to no. 1 cover glass. The surface of the device was functionalized with 0.01% poly-L-Lysine for 2 h, and 1% glutaraldehyde for 15 min. 160 μm acupuncture needles (Seirin) were loaded into the needle guides and devices were UV sterilized or 15 min. 2.5 mg/mL collagen gels were then prepared on ice by buffering rat tail collagen type I (BD Biosciences) with 10x reconstitution buffer (0.2 M HEPES, 0.02 M sodium bicarbonate) and 10× DMEM. One N NaOH was used to bring the pH of the solution to 7.5 and PBS was added to bring the final concentration to 2.5 mg/mL. 35 μL of collagen solution was added to one of the collagen ports of each device and devices were incubated at 37 °C for 30 min. Each device was washed with PBS overnight and needles were removed from each of the needle guides.

Light Plate Apparatus

The light plate apparatus was fabricated in-house to independently control 24 independent light-emitting diodes (LED) (3.4 V ultrabright 3 mm LEDs, Chanzon) in a standard 24-well plate format. We desired that each LED could be independently programmed to (a) vary the illumination intensity and (b) illumination duration. To these ends, and Arduino Nano Every microcontroller (Arduino) was employed in conjunction with a 24-Channel, pulse-width modulation (PWM) LED driver breakout board (Adafruit TLC5947PWM LED Driver Breakouts, Adafruit) to control each of the 24 LEDs independently. Desired illumination intensity and illumination duration of each LED was programmed and uploaded to the microcontroller using the Arduino integrated development environment (IDE). A momentary tactile push button was included in the setup to allow the user to initiate the sequence (i.e., when the user pushes the button, the internal timer initiates, and the LED ON/OFF sequence commences). An organic light-emitting diode (OLED) screen (SSD1306 0.96 in. I2C OLED, Amazon) was included in the setup to display the elapsed time after user. The 24 LEDs were mounted on a poly(methyl methacrylate) (PMMA) substrate that was laser-cut with guide holes to align each LED with the 24-well plate. A modified μ-Plate 24 Well Black (Ibidi) with the bottom coverslip removed was adhered on PMMA substrate to prevent illumination of one LED from affecting its neighboring wells.

Immunofluorescence Imaging

Fixation of devices or monolayers at the appropriate time points was achieved using a 4% paraformaldehyde (Electron Microscopy Sciences) solution in DMEM/F12. For 3D devices, this solution was infused into all media reservoirs for 30 min at 37 °C, followed by three washes with PBS at 37 °C. For monolayers, the media was added to each well and plates were placed on a rocker at 37 °C, for 15 min, followed by three 5 min washes in PBS. For both monolayers and devices, cells were permeabilized in 0.25% Triton-X (Sigma) for 30 min on a rocker at room temperature and then washed three times with PBS (30 min each). Samples were blocked overnight by rocking in a 2% BSA solution at 4 °C, and primary antibody staining was achieved by rocking overnight with primary antibody at specified concentration overnight at 4 °C. Samples were washed three times in PBS (30 min for devices, 5 min for monolayers) and were then treated with secondary antibody at stated dilution and rocked overnight at 4 °C. Samples were washed three times in PBS for 30 min each wash. Devices were then imaged on a Leica SP8 laser scanning confocal microscope (Leica Microsystems) with Leica HC FLUOTAR L 25×/0.95 W VISIR controlled by LASX software. 2D phase contrast and fluorescent images were collected on a Nikon Eclipse Ti inverted microscope using either a 4× Nikon, 10× Nikon or 20× Nikon Plan Apo objective controlled by Metamorph software (Molecular Devices). Fluorescence images were adjusted for contrast and brightness using ImageJ (NIH).

Antibodies and Reagents

Anti-HA (C29F4,#3724), anti-pAkt (Ser473) (#9271), HRP-conjugated donkey antimouse (#7076, HER2/ErbB2 (29D8, #2165) and anti-GAPDH (14C10, #2118) were purchased from Cell Signaling Technologies. DAPI was from Santa Cruz biotechnology. Alexa Fluor 647 conjugated rabbit and mouse secondary

https://doi.org/10.1021/acssynbio.5c00651
ACS Synth. Biol. XXXX, XXX, XXX−XXX

antibodies were from Life Technologies. Alexa Fluor Plus (488, 647) Phalloidin was purchased from Invitrogen. GDC0941 was purchased from Selleckchem.

RT-qPCR

MCF10A cells were seeded into a 6-well plate at a density of 200,000 cells per well and treated with 1 μg/mL of doxycycline or DMSO for 72 h. RNA was extracted by means of a phenol-chloroform extraction. Briefly, cells were lysed using 500 μL Trizol (Thermo Fisher Scientific), transferred to Eppendorf tubes, and 100 μL of chloroform was added to each tube. Cells were spun at 15,000 *g* for 20 min, and the supernatant was removed and transferred to an RNeasy Mini column (Qiagen). The RNeasy protocol was used to complete the RNA purification as per manufacturer's instructions. cDNA was then synthesized using the qScript cDNA SuperMix (VWR) as per kit instructions. cDNA was stored at −20 °C and thawed as needed.

To quantify transcript content, forward and reverse primers targeting the gene of interest were determined using a combination of literature review and NIH Primer Blast. PowerUP SYBR Green Master Mix (Thermo Fischer) was mixed with the forward and reverse primers and diluted as outlined on package instructions. 10 ng of RNA was added to each well of a 96 well plate, along with the appropriate amount of SYBR Green Master Mix and qPCR was run according to manufacturer's instructions. Quantification of fold change was performed using the delta−delta Ct method. Primers used for each analysis are outlined in Table 1.

Table 1

gene	forward primer	reverse primer
GAPDH	TCAAGGCTGAGAACG GGAAG	CGCCCCACTTGATTT TGGAG
TWIST1	GCAAGAAGTCGAGCG AAGAT	GCTCTGCAGC TCCTCGAA
SNAI1	TCGGAAGCCTAACTA CAGCGA	AGATGAGCATTGGCA GCGAG
SNAI2	CGAACTGGACACACA TACAGTG	CTGAGGATCTCTGGT TGTGGT
ZEB1	TTACACCTTTGCATA CAGAACCC	TTTACGATTACACCC AGACTGC
ZEB2	GGAGACGAGTCCAGC TAGTGT	CCACTCCACCCTCCC TTATTTC

Scratch Wound Assay

MCF10A cells were grown to a confluent monolayer in a 24 well plate. Using the tip of a P10 pipet, a line was carefully drawn across the midpoint of each well by pressing the tip into the cellular monolayer and dragging it along the plastic. Monolayers were washed twice with PBS and appropriate medium was added to each well. For the mutant migration studies, each wound was imaged in three distinct locations using a 10x objective on a Nikon Eclipse TI2 microscope (Nikon) and imaged every 15 min on an incubated stage. A custom CellProlifer script was used to identify the wound margin and quantify the degree of wound closure over time.[77]

For the optoPI3K experiments, each wound was imaged on the Nikon Eclipse Ti2 using a 4× objective immediately following the scratch. The plate was placed in a humidified incubator on a LED lightbox programmed to deliver a 30 min, 120 min or 24 h stimulus of blue light. 24 hours following the scratch, each well of the plate was imaged again. FIJI was used to measure the wound area immediately after the scratch and again following stimulation, and the degree of wound closure was quantified using the following formula:

$$\%\text{Closures} = 1 - \frac{\text{WoundArea}_{\text{Final}}}{\text{WoundArea}_{\text{Initial}}}$$

Cell Shape Analysis

Phase contrast images of WT, ErbB2^{amp}-expressing, PIK3CA^{H1047R}-expressing or OptoPI3K expressing MCF10A cells were collected using a 20× Nikon objective on a Nikon Eclipse Ti2 inverted microscope. More than 30 cells per image were manually outlined in FIJI, which was used to compute the cell area, circularity, and aspect ratio of each cell.

Signal Dynamic Analysis

MCF10A cells or cells expressing either mutation were grown to confluence in a 6 well dish using MCF10A growth medium. Monolayers were washed 3× with PBS and cultured for 24 h in 2 mL MCF10A starvation medium. For ligand stimulation assays, a 3× concentration solution in starvation medium solution was made—(EGF (15 ng/mL) or insulin (30 μg/mL)—and 1 mL of this fortified medium was added to the 2 mL starvation medium already in each well, such that the effective ligand concentration in each well became that found in normal MCF10A assay medium. Concentrated medium was serially added to wells in reverse chronological order, such that at the end of the experiment, protein could be harvested from all wells at once with various durations of stimulation collected. Stimulation was performed in duplicate wells, which were pools for analysis. Cell lysis and protein collection performed using standard Western Blotting protocol and RIPA buffer. For graphical display, everything was normalized to peak value to facilitate assessment of curve shape and duration.

Proliferation Assay

WT, ErbB2^{amp}-expressing and PI3K^{H1047R} expressing MCF10A cells were grown to confluence in a 24 well plate. Cells were starved overnight in starvation medium, after which time 5 ng/mL EGF and 5 μM Click-iT Plus Edu reagent (Thermo) were added to each well. Cells were grown for 24 h in the presence of the Edu before they were fixed. Cells were then permeabilized and treated per the product insert to drive the conjugation of AlexaFluor 647 to the Edu via Click chemistry. A similar protocol was utilized for the optoPI3K experiments, where optoPI3K expressing MCF10A cells were used in place of the mutant expressing MCF10A, and the individual mutant mimetic signals were used in place of EGF addition.

TCGA Gene Expression Analysis

The METABRIC TCGA breast cancer data set was mined using cBioPortal to compare expression levels of MKI67, Vim and CDH1 in patients with tumors harboring either the PI3K H1047R mutation (n = 360) or an *ErbB2* amplification (n = 319).[36,37,78,79] Plotting and statistics, including FDR, computed using cBioPortal analysis tools.

Statistical Analysis

Sample sizes and P values are reported in each of the figure legends. All statistical analysis was performed in GraphPad Prism 10, unless otherwise noted. Unless otherwise specified, multigroup analysis was performed using a one-way analysis of variance (ANOVA) with a Bonferroni posthoc test to report adjusted P values, while dual group analysis was performed using a two-tailed, unpaired Student's t test.

■ ASSOCIATED CONTENT

Data Availability Statement

The data that support the findings of this study are available upon reasonable request from the corresponding authors.

Supporting Information

The Supporting Information is available free of charge at https://pubs.acs.org/doi/10.1021/acssynbio.5c00651.

Supplemental Figure 1: Supplemental TGFb-mediated EMT data and raw signal dynamics data; Supplemental Figure 2: blue light stimulation of MCF10A does not negatively affect viability; Supplemental Figure 3: representative scratch wound closures in optogenetic stimulation; Supplemental Figure 4: raw blots used for OptoPI3K quantification (PDF)

https://doi.org/10.1021/acssynbio.5c00651
ACS Synth. Biol. XXXX, XXX, XXX−XXX

AUTHOR INFORMATION

Corresponding Authors

Ahmad S. Khalil − *Department of Biomedical Engineering and Biological Design Center, Boston University, Boston, Massachusetts 02215, United States; Wyss Institute for Biologically Inspired Engineering, Harvard University, Boston, Massachusetts 02115, United States;* orcid.org/0000-0002-8214-0546; Email: khalil@bu.edu

Christopher S. Chen − *Department of Biomedical Engineering and Biological Design Center, Boston University, Boston, Massachusetts 02215, United States; Wyss Institute for Biologically Inspired Engineering, Harvard University, Boston, Massachusetts 02115, United States;* orcid.org/0000-0003-2445-8449; Email: chencs@bu.edu

Authors

Keith A. Gagnon − *Department of Biomedical Engineering and Biological Design Center, Boston University, Boston, Massachusetts 02215, United States;* orcid.org/0000-0002-8898-9372

Veronica W. Hui − *Department of Biomedical Engineering, Boston University, Boston, Massachusetts 02215, United States; Harvard-MIT Division of Health Sciences and Technology, Institute for Medical Engineering and Science, Massachusetts Institute of Technology, Cambridge, Massachusetts 02139, United States*

Terry Ching − *Department of Biomedical Engineering and Biological Design Center, Boston University, Boston, Massachusetts 02215, United States; Wyss Institute for Biologically Inspired Engineering, Harvard University, Boston, Massachusetts 02115, United States*

Amy E. Stoddard − *Biological Design Center, Boston University, Boston, Massachusetts 02215, United States; Harvard-MIT Division of Health Sciences and Technology, Institute for Medical Engineering and Science, Massachusetts Institute of Technology, Cambridge, Massachusetts 02139, United States*

Esther Koh − *Biological Design Center, Boston University, Boston, Massachusetts 02215, United States; Harvard-MIT Division of Health Sciences and Technology, Institute for Medical Engineering and Science, Massachusetts Institute of Technology, Cambridge, Massachusetts 02139, United States*

Jeroen Eyckmans − *Department of Biomedical Engineering and Biological Design Center, Boston University, Boston, Massachusetts 02215, United States; Wyss Institute for Biologically Inspired Engineering, Harvard University, Boston, Massachusetts 02115, United States*

Complete contact information is available at: https://pubs.acs.org/10.1021/acssynbio.5c00651

Author Contributions

K.A.G: Conceptualization, methodology, investigation, validation, formal analysis, writing—original draft, writing—reviewing and editing, visualization, funding acquisition; V.W.H.: Methodology, investigation, validation, formal analysis, writing—reviewing and editing; T.C: Methodology, investigation, writing—reviewing and editing; A.E.S: Methodology, investigation, writing—reviewing and editing; E.K.: Methodology, investigation; J.E: Writing—reviewing and editing, supervision; A.S.K: Conceptualization, methodology, writing—reviewing and editing, visualization, supervision, funding acquisition; C.S.C: Conceptualization, methodology, writing—reviewing and editing, supervision, funding acquisition.

Notes

No ethics approval was required for the experiments described in this study.

The authors declare the following competing financial interest(s): A.S.K. is a scientific advisor for and holds equity in Senti Biosciences and nChroma Bio and is a cofounder of K2 Therapeutics. C.S.C. is a founder and owns shares of Satellite Biosciences and Ropirio Therapeutics. None of these companies have interests in relation to the current study.

ACKNOWLEDGMENTS

This work was supported by the National Institutes of Health (NIH) (Grant Nos. R01EB033821 to C.S.C. and A.S.K.; R01EB029483 to A.S.K.; T32HL007035 to K.A.G), the National Science Foundation Science and Technology Center for Engineering Mechanobiology (CMMI-1548571 to C.S.C.), the Department of Defense Vannevar Bush Faculty Fellowship (No. N00014-20-1-2825 to A.S.K.), and The Paul G. Allen Distinguished Investigator award (to C.S.C.). The results shown here are in part based upon data generated by the TCGA Research Network: https://www.cancer.gov/tcga, and analyzed using the cBioPortal platform (https://www.cbioportal.org/).

REFERENCES

(1) Lemmon, M. A.; Schlessinger, J. Cell Signaling by Receptor Tyrosine Kinases. *Cell* **2010**, *141*, 1117−1134.

(2) Wu, H. Higher-Order Assemblies in a New Paradigm of Signal Transduction. *Cell* **2013**, *153*, 287−292.

(3) Kholodenko, B. N. Cell-signalling dynamics in time and space. *Nat. Rev. Mol. Cell Biol.* **2006**, *7*, 165−176.

(4) Sonnen, K. F.; Aulehla, A. Dynamic signal encoding–from cells to organisms. *Semin. Cell Dev. Biol.* **2014**, *34*, 91−98.

(5) Antebi, Y. E.; Linton, J. M.; Klumpe, H.; Bintu, B.; Gong, M.; Su, C.; McCardell, R.; Elowitz, M. B. Combinatorial signal perception in the BMP pathway. *Cell* **2017**, *170*, 1184−1196.

(6) Nandagopal, N.; Santat, L. A.; LeBon, L.; Sprinzak, D.; Bronner, M. E.; Elowitz, M. B. Dynamic Ligand Discrimination in the Notch Signaling Pathway. *Cell* **2018**, *172*, 869−880.e19.

(7) Purvis, J. E.; Lahav, G. Encoding and decoding cellular information through signaling dynamics. *Cell* **2013**, *152*, 945−956.

(8) Li, P.; Elowitz, M. B.; Klein, A.; Treutlein, B. Communication codes in developmental signaling pathways. *Development* **2019**, *146*, dev170977.

(9) Batchelor, E.; Loewer, A.; Mock, C.; Lahav, G. Stimulus-dependent dynamics of p53 in single cells. *Mol. Syst. Biol.* **2011**, *7*, 488.

(10) Lahav, G.; Rosenfeld, N.; Sigal, A.; Geva-Zatorsky, N.; Levine, A. J.; Elowitz, M. B.; Alon, U. Dynamics of the p53-Mdm2 feedback loop in individual cells. *Nat. Genet.* **2004**, *36*, 147−150.

(11) Marshall, C. J. Specificity of receptor tyrosine kinase signaling: Transient versus sustained extracellular signal-regulated kinase activation. *Cell* **1995**, *80*, 179−185.

(12) Hanahan, D. Hallmarks of cancer: new dimensions. *Cancer Discovery* **2022**, *12*, 31−46.

(13) Hanahan, D.; Weinberg, R. A. Hallmarks of cancer: The next generation. *Cell* **2011**, *144*, 646−674.

(14) Hanahan, D.; Weinberg, R. A. The hallmarks of cancer. *Cell* **2000**, *100*, 57−70.

(15) Hobbs, G. A.; Der, C. J.; Rossman, K. L. RAS isoforms and mutations in cancer at a glance. *J. Cell Sci.* **2016**, *129*, 1287−1292.

(16) Ihle, N. T.; Byers, L. A.; Kim, E. S.; Saintigny, P.; Lee, J. J.; Blumenschein, G. R.; Tsao, A.; Liu, S.; Larsen, J. E.; Wang, J.; Diao, L.; Coombes, K. R.; Chen, L.; Zhang, S.; Abdelmelek, M. F.; Tang, X.;

Papadimitrakopoulou, V.; Minna, J. D.; Lippman, S. M.; Hong, W. K.; Herbst, R. S.; Wistuba, I. I.; Heymach, J. V.; Powis, G. Effect of KRAS oncogene substitutions on protein behavior: implications for signaling and clinical outcome. *J. Natl. Cancer Inst.* **2012**, *104*, 228−239.
(17) Vogelstein, B.; Papadopoulos, N.; Velculescu, V. E.; Zhou, S.; Diaz, L. A.; Kinzler, K. W. Cancer Genome Landscapes. *Science (80-.)* **2013**, *339*, 1546−1558.
(18) Bugaj, L. J.; Sabnis, A. J.; Mitchell, A.; Garbarino, J. E.; Toettcher, J. E.; Bivona, T. G.; Lim, W. A. Cancer mutations and targeted drugs can disrupt dynamic signal encoding by the Ras-Erk pathway. *Science (80-.)* **2018**, *361*, No. eaao3048.
(19) Fayard, E.; Xue, G.; Parcellier, A.; Bozulic, L.; Hemmings, B. A.; Rommel, C.; Vanhaesebroeck, B.; Vogt, P. K. Protein kinase B (PKB/Akt), a key mediator of the PI3K signaling pathway. *Curr. Top. Microbiol. Immunol.* **2010**, *346*, 31−56.
(20) Martini, M.; De Santis, M. C.; Braccini, L.; Gulluni, F.; Hirsch, E. PI3K/AKT signaling pathway and cancer: an updated review. *Ann. Med.* **2014**, *46*, 372−383.
(21) Wong, K.-K.; Engelman, J. A.; Cantley, L. C. Targeting the PI3K signaling pathway in cancer. *Curr. Opin. Genet. Dev.* **2010**, *20*, 87−90.
(22) Tengholm, A.; Meyer, T. A PI3-Kinase Signaling Code for Insulin-Triggered Insertion of Glucose Transporters into the Plasma Membrane. *Curr. Biol.* **2002**, *12*, 1871−1876.
(23) Kubota, H.; Noguchi, R.; Toyoshima, Y.; Ozaki, Y.-I.; Uda, S.; Watanabe, K.; Ogawa, W.; Kuroda, S. Temporal coding of insulin action through multiplexing of the AKT pathway. *Mol. Cell* **2012**, *46*, 820−832.
(24) Kubota, H.; Uda, S.; Matsuzaki, F.; Yamauchi, Y.; Kuroda, S. In Vivo Decoding Mechanisms of the Temporal Patterns of Blood Insulin by the Insulin-AKT Pathway in the Liver. *Cell Syst.* **2018**, *7*, 118−128.e3.
(25) Gross, S. M.; Dane, M. A.; Bucher, E.; Heiser, L. M. Individual Cells Can Resolve Variations in Stimulus Intensity along the IGF-PI3K-AKT Signaling Axis. *Cell Syst.* **2019**, *9*, 580−588.e4.
(26) Gross, S. M.; Rotwein, P. Akt signaling dynamics in individual cells. *J. Cell Sci.* **2015**, *128*, 2509−2519.
(27) Gross, S. M.; Rotwein, P. Mapping growth-factor-modulated Akt signaling dynamics. *J. Cell Sci.* **2016**, *129*, 2052−2063.
(28) Gagliardi, P. A.; Dobrzyński, M.; Jacques, M. A.; Dessauges, C.; Ender, P.; Blum, Y.; Hughes, R. M.; Cohen, A. R.; Pertz, O. Collective ERK/Akt activity waves orchestrate epithelial homeostasis by driving apoptosis-induced survival. *Dev. Cell* **2021**, *56*, 1712−1726.e6.
(29) Miller, T. W.; Rexer, B. N.; Garrett, J. T.; Arteaga, C. L. Mutations in the phosphatidylinositol 3-kinase pathway: Role in tumor progression and therapeutic implications in breast cancer. *Breast Cancer Res.* **2011**, *13*, 224.
(30) The Cancer Genome Atlas. (**2012**) Comprehensive molecular portraits of human breast tumours. *Nature 490*, 61−70.
(31) Yuan, T. L.; Wulf, G.; Burga, L.; Cantley, L. C. Cell-to-cell variability in PI3K protein level regulates PI3K-AKT pathway activity in cell populations. *Curr. Biol.* **2011**, *21*, 173−183.
(32) Kutys, M. L.; Polacheck, W. J.; Welch, M. K.; Gagnon, K. A.; Koorman, T.; Kim, S.; Li, L.; McClatchey, A. I.; Chen, C. S. Uncovering mutation-specific morphogenic phenotypes and paracrine-mediated vessel dysfunction in a biomimetic vascularized mammary duct platform. *Nat. Commun.* **2020**, *11*, 3377.
(33) Ruiz-Saenz, A.; Dreyer, C.; Campbell, M. R.; Steri, V.; Gulizia, N.; Moasser, M. M. HER2 Amplification in Tumors Activates PI3K/Akt Signaling Independent of HER3. *Cancer Res.* **2018**, *78*, 3645−3658.
(34) He, Y.; Sun, M. M.; Zhang, G. G.; Yang, J.; Chen, K. S.; Xu, W. W.; Li, B. Targeting PI3K/Akt signal transduction for cancer therapy. *Signal Transduct. Target. Ther.* **2021**, *6*, 425.
(35) Hynes, N. E.; MacDonald, G. ErbB receptors and signaling pathways in cancer. *Curr. Opin. Cell Biol.* **2009**, *21*, 177−184.
(36) Curtis, C.; Shah, S. P.; Chin, S. F.; Turashvili, G.; Rueda, O. M.; Dunning, M. J.; Speed, D.; Lynch, A. G.; Samarajiwa, S.; Yuan, Y.; Gräf, S.; Ha, G.; Haffari, G.; Bashashati, A.; Russell, R.; McKinney, S.; Langerød, A.; Green, A.; Provenzano, E.; Wishart, G.; Pinder, S.; Watson, P.; Markowetz, F.; Murphy, L.; Ellis, I.; Purushotham, A.; Børresen-Dale, A. L.; Brenton, J. D.; Tavaré, S.; Caldas, C.; Aparicio, S. The genomic and transcriptomic architecture of 2,000 breast tumours reveals novel subgroups. *Nature* **2012**, *486*, 346−352.
(37) Pereira, B.; Chin, S. F.; Rueda, O. M.; Vollan, H. K. M.; Provenzano, E.; Bardwell, H. A.; Pugh, M.; Jones, L.; Russell, R.; Sammut, S. J.; Tsui, D. W. Y.; Liu, B.; Dawson, S. J.; Abraham, J.; Northen, H.; Peden, J. F.; Mukherjee, A.; Turashvili, G.; Green, A. R.; McKinney, S.; Oloumi, A.; Shah, S.; Rosenfeld, N.; Murphy, L.; Bentley, D. R.; Ellis, I. O.; Purushotham, A.; Pinder, S. E.; Børresen-Dale, A. L.; Earl, H. M.; Pharoah, P. D.; Ross, M. T.; Aparicio, S.; Caldas, C. The somatic mutation profiles of 2433 breast cancers refine their genomic and transcriptomic landscapes. *Nat. Commun.* **2016**, *7*, 11479.
(38) Miron, K.; Golan-Lev, T.; Dvir, R.; Ben-David, E.; Kerem, B. Oncogenes create a unique landscape of fragile sites. *Nat. Commun.* **2015**, *6*, 7094.
(39) Moreno-Bueno, G.; Peinado, H.; Molina, P.; Olmeda, D.; Cubillo, E.; Santos, V.; Palacios, J.; Portillo, F.; Cano, A. The morphological and molecular features of the epithelial-to-mesenchymal transition. *Nat. Protoc.* **2009**, *4*, 1591−1613.
(40) Nurmagambetova, A.; Mustyatsa, V.; Saidova, A.; Vorobjev, I. Morphological and cytoskeleton changes in cells after EMT. *Sci. Rep.* **2023**, *13*, 22164.
(41) Zhang, J.; Tian, X. J.; Zhang, H.; Teng, Y.; Li, R.; Bai, F.; Elankumaran, S.; Xing, J. TGF-β-induced epithelial-to-mesenchymal transition proceeds through stepwise activation of multiple feedback loops. *Sci. Signal.* **2014**, *7*, ra91.
(42) Carmona, F. J.; Montemurro, F.; Kannan, S.; Rossi, V.; Verma, C.; Baselga, J.; Scaltriti, M. AKT signaling in ERBB2-amplified breast cancer. *Pharmacol. Ther.* **2016**, *158*, 63−70.
(43) Miller, T. W. Initiating breast cancer by PIK3CA mutation. *Breast Cancer Res.* **2012**, *14*, 301.
(44) Bugaj, L. J.; Lim, W. A. High-throughput multicolor optogenetics in microwell plates. *Nat. Protoc.* **2019**, *14*, 2205−2228.
(45) Town, J. P.; Weiner, O. D. Local negative feedback of Rac activity at the leading edge underlies a pilot pseudopod-like program for amoeboid cell guidance. *PLoS Biol.* **2023**, *21*, No. e3002307.
(46) Ueda, Y.; Miura, Y.; Tomishige, N.; Sugimoto, N.; Murase, M.; Kawamura, G.; Sasaki, N.; Ishiwata, T.; Ozawa, T. Mechanistic insights into cancer drug resistance through optogenetic PI3K signaling hyperactivation. *Cell Chem. Biol.* **2022**, *29*, 1576−1587.e5.
(47) Toettcher, J. E.; Gong, D.; Lim, W. A.; Weiner, O. D. Light-based feedback for controlling intracellular signaling dynamics. *Nat. Methods* **2011**, *8*, 837−839.
(48) Guntas, G.; Hallett, R. A.; Zimmerman, S. P.; Williams, T.; Yumerefendi, H.; Bear, J. E.; Kuhlman, B. Engineering an improved light-induced dimer (iLID) for controlling the localization and activity of signaling proteins. *Proc. Natl. Acad. Sci. U. S. A.* **2015**, *112*, 112−117.
(49) Klewer, L.; Wu, Y. W. Light-Induced Dimerization Approaches to Control Cellular Processes. *Chem. - A Eur. J.* **2019**, *25*, 12452−12463.
(50) Idevall-Hagren, O.; Dickson, E. J.; Hille, B.; Toomre, D. K.; De Camilli, P. Optogenetic control of phosphoinositide metabolism. *Proc. Natl. Acad. Sci. U. S. A.* **2012**, *109*, E2316−E2323.
(51) Suh, B.-C.; Inoue, T.; Meyer, T.; Hille, B. Rapid chemically induced changes of PtdIns(4,5)P2 gate KCNQ ion channels. *Science* **2006**, *314*, 1454−1457.
(52) Xu, Y.; Nan, D.; Fan, J.; Bogan, J. S.; Toomre, D. Optogenetic activation reveals distinct roles of PIP3 and Akt in adipocyte insulin action. *J. Cell Sci.* **2016**, *129*, 2085−2095.
(53) Koh, D.-S.; Stratiievska, A.; Jana, S.; Otto, S. C.; Swanson, T. M.; Nhim, A.; Carlson, S.; Raza, M.; Naves, L. A.; Senning, E. N.; Mehl, R. A.; Gordon, S. E. Genetic code expansion, click chemistry, and light-activated PI3K reveal details of membrane protein trafficking downstream of receptor tyrosine kinases. *Elife* **2024**, *12*, RP91012.

https://doi.org/10.1021/acssynbio.5c00651
ACS Synth. Biol. XXXX, XXX, XXX−XXX

(54) Lauring, J.; Cosgrove, D. P.; Fontana, S.; Gustin, J. P.; Konishi, H.; Abukhdeir, A. M.; Garay, J. P.; Mohseni, M.; Wang, G. M.; Higgins, M. J.; Gorkin, D.; Reis, M.; Vogelstein, B.; Polyak, K.; Cowherd, M.; Buckhaults, P. J.; Park, B. H. Knock in of the AKT1 E17K mutation in human breast epithelial cells does not recapitulate oncogenic PIK3CA mutations. *Oncogene* **2010**, *29*, 2337−2345.
(55) Beaver, J. A.; Gustin, J. P.; Yi, K. H.; Rajpurohit, A.; Thomas, M.; Gilbert, S. F.; Rosen, D. M.; Ho Park, B.; Lauring, J. PIK3CA and AKT1 mutations have distinct effects on sensitivity to targeted pathway inhibitors in an isogenic luminal breast cancer model system. *Clin. cancer Res. an Off. J. Am. Assoc. Cancer Res.* **2013**, *19*, 5413−5422.
(56) Gjelaj, E.; Hamel, P. A. Distinct epithelial-to-mesenchymal transitions induced by PIK3CA H1047R and PIK3CB. *J. Cell Sci.* **2021**, *134*, jcs248294.
(57) Zafra, M. P.; Parsons, M. J.; Kim, J.; Alonso-Curbelo, D.; Goswami, S.; Schatoff, E. M.; Han, T.; Katti, A.; Fernandez, M. T. C.; Wilkinson, J. E.; Piskounova, E.; Dow, L. E. An In Vivo Kras Allelic Series Reveals Distinct Phenotypes of Common Oncogenic Variants. *Cancer Discovery* **2020**, *10*, 1654−1671.
(58) Inoue, T.; Meyer, T. Synthetic Activation of Endogenous PI3K and Rac Identifies an AND-Gate Switch for Cell Polarization and Migration. *PLoS One* **2008**, *3*, No. e3068.
(59) Feng, S.; Laketa, V.; Stein, F.; Rutkowska, A.; MacNamara, A.; Depner, S.; Klingmüller, U.; Saez-Rodriguez, J.; Schultz, C. A rapidly reversible chemical dimerizer system to study lipid signaling in living cells. *Angew. Chem.* **2014**, *126*, 6838−6841.
(60) Kwon, E.; Heo, W. Do Optogenetic tools for dissecting complex intracellular signaling pathways. *Biochem. Biophys. Res. Commun.* **2020**, *527*, 331−336.
(61) Toettcher, J. E.; Weiner, O. D.; Lim, W. A. Using optogenetics to interrogate the dynamic control of signal transmission by the Ras/Erk module. *Cell* **2013**, *155*, 1422−1434.
(62) Tsuruoka, T.; Goto, Y.; Aoki, K. Opto-p53: A light-controllable activation of p53 signaling pathway. *Cell Struct. Funct.* **2025**, *50*, 145−156.
(63) Katsura, Y.; Kubota, H.; Kunida, K.; Kanno, A.; Kuroda, S.; Ozawa, T. An optogenetic system for interrogating the temporal dynamics of Akt. *Sci. Rep.* **2015**, *5*, No. 14589.
(64) Meyer, K.; Lammers, N. C.; Bugaj, L. J.; Garcia, H. G.; Weiner, O. D. Optogenetic control of YAP reveals a dynamic communication code for stem cell fate and proliferation. *Nat. Commun.* **2023**, *14*, 6929.
(65) Kim, N.; Kim, J. M.; Heo, W. Do Optogenetic Control of Fibroblast Growth Factor Receptor Signaling. *Methods Mol. Biol.* **2016**, *1408*, 345−362.
(66) Zhang, K.; Cui, B. Optogenetic control of intracellular signaling pathways. *Trends Biotechnol.* **2015**, *33*, 92−100.
(67) Xu, W.; Yang, Z.; Lu, N. A new role for the PI3K/Akt signaling pathway in the epithelial-mesenchymal transition. *Cell Adh. Migr.* **2015**, *9*, 317−324.
(68) Maharati, A.; Moghbeli, M. PI3K/AKT signaling pathway as a critical regulator of epithelial-mesenchymal transition in colorectal tumor cells. *Cell Commun. Signal.* **2023**, *21*, 201.
(69) Moghbeli, M. PI3K/AKT pathway as a pivotal regulator of epithelial-mesenchymal transition in lung tumor cells. *Cancer Cell Int.* **2024**, *24*, 165.
(70) Zhou, X.; Wang, J.; Chen, J.; Qi, Y.; Nan, D.; Jin, L.; Qian, X.; Wang, X.; Chen, Q.; Liu, X.; Xu, Y. Optogenetic control of epithelial-mesenchymal transition in cancer cells. *Sci. Rep.* **2018**, *8*, 14098.
(71) Madsen, R. R.; Le Marois, A.; Mruk, O. N.; Voliotis, M.; Yin, S.; Sufi, J.; Qin, X.; Zhao, S. J.; Gorczynska, J.; Morelli, D.; Davidson, L.; Sahai, E.; Korolchuk, V. I.; Tape, C. J.; Vanhaesebroeck, B. Oncogenic PIK3CA corrupts growth factor signaling specificity. *Mol. Syst. Biol.* **2024**, *21*, 126−157.
(72) Chaffer, C.; Weinberg, R. A Perspective on Cancer Cell Metastasis. *Science (80-.).* **2011**, *331*, 1559−1565.
(73) Simond, A. M.; Bui, T.; Zuo, D.; Sanguin-Gendreau, V.; Rao, T.; Phillips, W. A.; Cardiff, R. D.; Muller, W. J. Physiological expression of PI3K H1047R mutation reveals its anti-metastatic potential in ErbB2-driven breast cancer. *Oncogene* **2022**, *41*, 3445−3451.
(74) Jeknić, S.; Kudo, T.; Covert, M. W. Techniques for studying decoding of single cell dynamics. *Front. Immunol.* **2019**, *10*, 755.
(75) Debnath, J.; Mills, K. R.; Collins, N. L.; Reginato, M. J.; Muthuswamy, S. K.; Brugge, J. S. The role of apoptosis in creating and maintaining luminal space within normal and oncogene-expressing mammary acini. *Cell* **2002**, *111*, 29−40.
(76) Muranen, T.; Iwanicki, M. P.; Curry, N. L.; Hwang, J.; DuBois, C. D.; Coloff, J. L.; Hitchcock, D. S.; Clish, C. B.; Brugge, J. S.; Kalaany, N. Y. Starved epithelial cells uptake extracellular matrix for survival. *Nat. Commun.* **2017**, *8*, No. 13989.
(77) Stirling, D. R.; Swain-Bowden, M. J.; Lucas, A. M.; Carpenter, A. E.; Cimini, B. A.; Goodman, A. CellProfiler 4: improvements in speed, utility and usability. *BMC Bioinf.* **2021**, *22*, 433.
(78) Cerami, E.; Gao, J.; Dogrusoz, U.; Gross, B. E.; Sumer, S. O.; Aksoy, B. A.; Jacobsen, A.; Byrne, C. J.; Heuer, M. L.; Larsson, E.; Antipin, Y.; Reva, B.; Goldberg, A. P.; Sander, C.; Schultz, N. The cBio cancer genomics portal: an open platform for exploring multidimensional cancer genomics data. *Cancer Discovery* **2012**, *2*, 401−404.
(79) Gao, J.; Aksoy, B. A.; Dogrusoz, U.; Dresdner, G.; Gross, B.; Sumer, S. O.; Sun, Y.; Jacobsen, A.; Sinha, R.; Larsson, E.; Cerami, E.; Sander, C.; Schultz, N. Integrative analysis of complex cancer genomics and clinical profiles using the cBioPortal. *Sci. Signal.* **2013**, *6*, pl1.

https://doi.org/10.1021/acssynbio.5c00651
ACS Synth. Biol. XXXX, XXX, XXX−XXX